Deep Learning and Density Functional Theory

Kevin Ryczko
Department of Physics
University of Ottawa
`kryczko@uottawa.ca`

David Strubbe
Department of Physics
University of California, Merced
`dstrubbe@ucmerced.edu`

Isaac Tamblyn
National Research Council of Canada
Department of Physics, University of Ottawa
Department of Physics, University of Ontario Institute of Technology
`isaac.tamblyn@nrc.ca`

Abstract

Density functional theory (DFT) is used for quantum mechanical simulations of electrons in molecules and materials, for applications in chemistry, physics, materials science, and engineering. However, usage of DFT for large numbers of atoms is hindered by typical scaling of $\mathcal{O}(N^3)$. Demonstration of a sufficiently accurate reduced model with deep neural networks would enable widespread application of DFT on larger, more complex systems for new scientific discoveries. We show that deep neural networks can be integrated into, or fully replace, the Kohn-Sham density functional theory scheme for multi-electron systems in simple harmonic oscillator and random external potentials. We first show that self-consistent charge densities can be used as input to an extensive deep neural network to make predictions for correlation, exchange, external, kinetic and total energies *simultaneously*. Additionally, we show that one can also make all of the same predictions with the external potential rather than the self-consistent charge density, which allows one to circumvent the Kohn-Sham scheme altogether. We then show that a self-consistent charge density found from a non-local exchange-correlation functional can be used to make energy predictions for a semi-local exchange-correlation functional. Lastly, we use a deep convolutional inverse graphics network to predict the charge density given an external potential and asses the viability of the predicted charge densities. This work shows that extensive deep neural networks are generalizable and transferable given the variability of the potentials and the fact that they can scale to an arbitrary system size with an $\mathcal{O}(N)$ computational cost.

1 Introduction

Kohn-Sham (KS) density functional theory (DFT)[1] is the standard tool to study nanoscale systems. Despite its success, DFT calculations for atomistic systems containing tens of thousands to millions of atoms are exceptionally demanding from a computational perspective and are rare in the literature. In recent literature, it has been suggested that machine learning techniques can replace conventional DFT calculations to overcome this computational barrier. Machine learning models are ideal because they rival the accuracy of the method they are trained on, but can be less demanding to evaluate from a computational standpoint. Evaluating a neural network is an $\mathcal{O}(N)$ task whereas electronic structure problems usually scale as $\mathcal{O}(N^3)$ or worse. There have been many reports where artificial neural networks (ANNs) have been used to represent potential energy surfaces to accelerate electronic structure calculations [2, 3, 4, 5, 6, 7, 8, 9]. These reports focus on feature engineering or defining
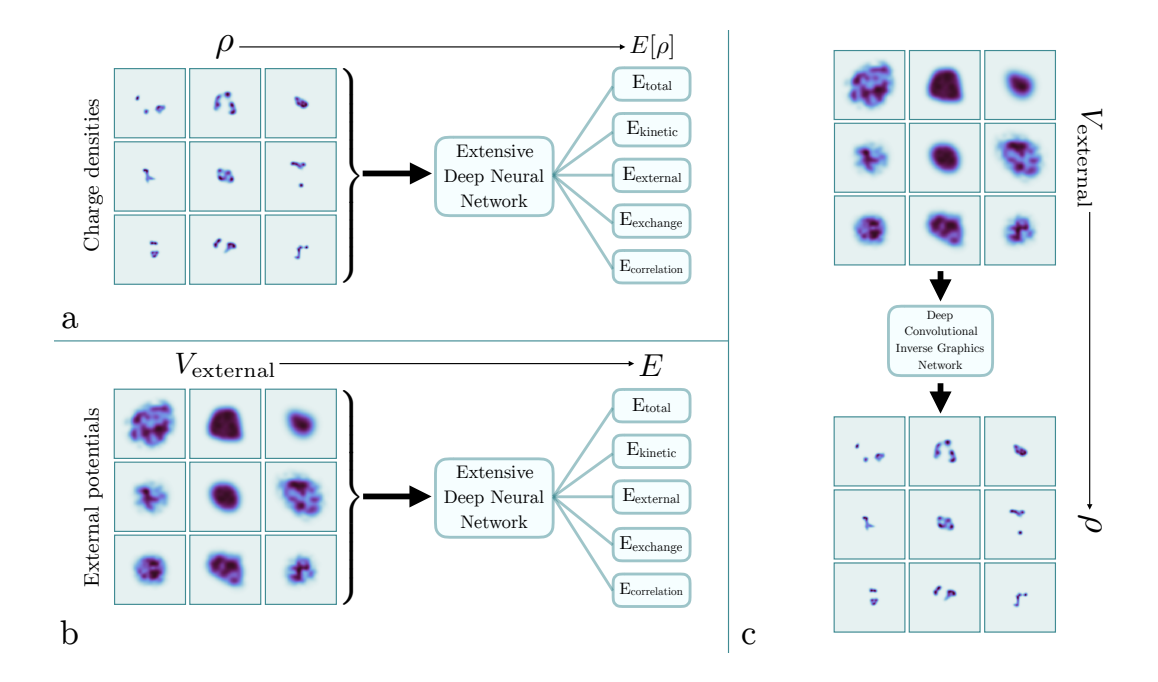
Figure 1: A graphical representation that outlines the objectives of this report. In a. and b. we show that both charge densities and external potentials can be used as input to extensive deep neural networks (EDNNs) to predict the total, kinetic, external, exchange and correlation energies. The images shown are some of the random (RND) potentials along with the self-consistent charge density for that potential. In c. we show that deep convolutional inverse graphics networks (DCIGNs) can be used to map external potentials to their respective self-consistent charge densities.

some abstract representation of atomistic systems allowing one to use an ANN. Instead, we focus our review on reports that avoid feature engineering and utilize the electron density in conjunction with machine learning. More specifically, machine learning has become a popular choice to represent energy functionals in DFT [10, 11, 12, 13, 14], or to completely circumvent the KS scheme [15, 16]. In deep learning, where the machine learning model learns the hierarchical features during training rather than inputing abstract representations there is a caveat for the previous statement. Due to the large number of tuneable parameters in deep neural networks (DNNs) that may include a variety of layers (i.e. convolutional, fully connected, max pooling, etc.), there must be thousands (if not hundreds of thousands) of training examples to find a stable minima with an acceptable accuracy. Generating these training examples is a computationally expensive task, but a trained DNN can evaluate a given quantity at a fraction of a cost compared to the original method.

An alternative, novel approach that has been taken recently by Brockherde *et al.* [15] is to focus more on uniformly sampling the space that a machine learning model will eventually predict and to use traditional machine learning with far fewer tuneable parameters. This approach was successful in predicting KS-DFT total energies and charge densities in one dimension (1D) for random Gaussian potentials and for small molecules in three dimensions (3D). Additionally, their training sets only consisted of a few hundred examples.

In KS-DFT, one of the contributions to the total energy is the non-interacting kinetic energy. Before the KS scheme was realized, Hohenberg and Kohn [17] postulated the formalism for an interacting kinetic energy functional of the density. To this day, an analytic expression for the exact interacting kinetic energy functional with respect to the electron density is unknown. This is one of the major downfalls of orbital-free (OF) DFT, where all energy contributions are explicitly written in terms of the electron density. This shortcoming provides motivation to construct an approximate functional of the density with a machine learning model. In a report done by Yao *et al.* [18], a convolutional neural network (CNN) was used to represent the kinetic energy functional in the OF-DFT total energy expression for various hydrocarbons. Their data generation process consisted of performing KS-DFT and collecting the charge density along with the KS non-interacting kinetic energy. The charge

density was then used as input to the CNN with the KS non-interacting kinetic energy as the label. With this representation they were able to successfully reproduce potential energy surfaces when compared to the true KS potential energy surfaces. In another report by Snyder *et al.* [13], they were able to use a machine learning model to make kinetic energy predictions given a charge density for a diatomic molecule. Using their framework, they were able to accurately dissociate the diatomic molecule, and compute forces suggesting that *ab initio* molecular dynamics could eventually be done via machine learning methods.

When representing the kinetic energy with a machine learning model in the OF scheme, one then becomes concerned with calculating the functional derivative of the machine learning model with respect to the density. In a report from Li *et al.* [12], they showed there is a trade off between accuracy and numerical noise to when taking the functional derivative of a machine learning model. Brockherde *et al.* [15] avoided this issue by training a machine learning model to learn the mapping between the potential and the electron density, avoiding the functional derivative.

In another recent report by Kolb *et al.* [14], a software package was developed to combine artificial neural networks with electronic structure calculations and molecular dynamics engines. Using their newly developed software, they were able to show that artificial neural networks can be used to make predictions with the electronic charge density as input and various energies as output. Specifically, they were able to predict energies and band gaps calculated at a higher level of theory from charge densities calculated at a lower level of theory. This approach is very advantageous as high level theory calculations (i.e. G_0W_0) become quite computationally expensive for larger systems.

Although significant progress has been made incorporating machine learning and deep learning to a variety of electronic structure problems, most do not have the ability to properly handle extensive properties. In some of our past work, extensive DNNs (EDNNs) [19] were introduced to intrinsically learn extensive properties. This means that when the DNN learns the fundamental screening length scale it can then easily scale up to massive systems in a trivially parallel manner. EDNNs work by first dividing up an image into fragments which are called focus regions. These fragments are then padded with context regions. The context regions may also respect periodic boundary conditions. Each of these fragments can then be simultaneously forward passed into a machine learning models that share weights. It should be noted here that any machine learning method that uses back propagation to minimize the loss function can be used. Finally, the outputs of the machine learning models are then summed yielding the final prediction from the EDNN.

In this report, we show that EDNNs have the capability to learn energy and charge density mappings that could replace some, if not all, calculations in KS-DFT scheme. We push the frontier of what EDNNs can learn from charge densities and external potentials by calculating the self-consistent charge densities in external potentials with extreme variabilities. In previous reports that focus on small molecules [15, 5, 14, 18], the self-consistent charge densities would have very similar structure for each configuration. We avoid small molecules (where the charge density would be localized in space), and truly challenge the ability of EDNNs to make accurate predictions across a variety of electronic environments. This report is outlined as follows: In Section 2, we describe our data generation process, as well as the DNN topologies and hyper-parameter selections. In Subsection 3.1, we show that DNNs have the capability to act as density functionals and can accurately predict the exchange, correlation, external, kinetic, and total energies *simultaneously* (Subsection 3.1.1). We also show that EDNNs can also circumvent the KS scheme (Subsection 3.1.2) by mapping the external potential to all of the aforementioned energies simultaneously. Additionally, we show that EDNNs can be used in a somewhat "perturbative" manner, where we predict energies computed with semi-local or non-local exchange-correlation functionals from non-local electron densities. In Subsection 3.2, we show that deep convolutional inverse graphics networks (DCIGNs) can also map the external potential to the electron density, and assess the viability of the predicted electron density. Lastly, in Section 4, we summarize our results and consider future work that could be done with our new framework. The outline of this manuscript can be seen graphically in Figure 1.

2 Methods

We investigate two-dimensional (2D) electron gases within the Kohn-Sham DFT framework [1] for two external potentials: the simple harmonic oscillator (SHO) and random (RND) potentials. These potentials have been used in a previous study [20] for exact, one-electron calculations. In the
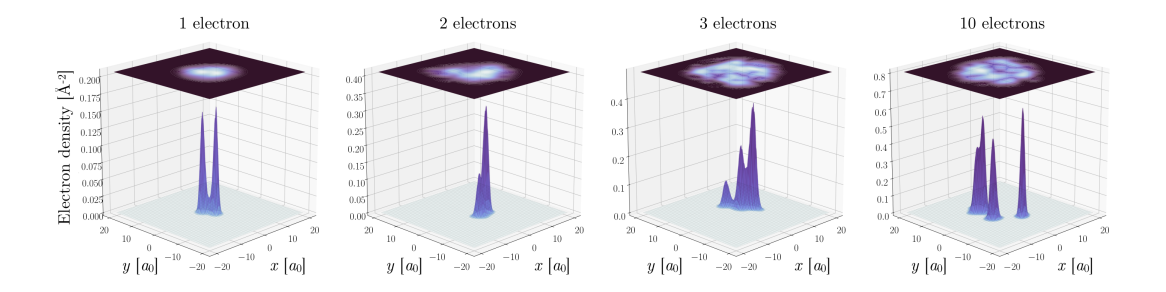
Figure 2: Computed charge densities (3D surfaces) and simple harmonic potential energy surfaces (2D surfaces) for randomly chosen configurations of systems with 1, 2, 3, and 10 electrons.

Kohn-sham DFT framework, one minimizes the total energy functional

$$E[n] = T[n] + E_{ext}[n] + E_{Hartree}[n] + E_{XC}[n] \tag{1}$$

which leads to the expression

$$E[n(\mathbf{r})] = \sum_i^{N/2} \epsilon_i - \frac{1}{2} \int \int d\mathbf{r} d\mathbf{r}' \frac{n(\mathbf{r})n(\mathbf{r}')}{|\mathbf{r} - \mathbf{r}'|} + E_{XC}[n] - \int d\mathbf{r} \, V_{XC}(n(\mathbf{r}))n(\mathbf{r}). \tag{2}$$

In Equation 1, T is the non-interacting kinetic energy functional, E_{ext} is the energy due to the interaction of the electrons with the external potential, $E_{Hartree}$ is the electrostatic energy describing the electron-electron interactions, and E_{XC} is the exchange-correlation energy.

With the EDNNs, we investigate the feasibility of learning the total energy as well as the individual contributions to the total energy. We therefore have trained models to predict the total, non-interacting kinetic, external, exchange, and correlation energies. The external potentials chosen for this report, as mentioned previously, are SHO and RND potentials in 2D. The SHO potentials take the form

$$V_{ext}(\{x_i\}) = \frac{1}{2} \sum_i^D k_i (x_i - x_{0_i})^2 \tag{3}$$

where D is the dimension, $k_i = m\omega_i^2$ is the spring constant, and x_{0_i} is the shift of the potential in a given coordinate. For the RND potentials we follow the work of Mills *et al.* [20] when generating the potentials on a grid. We refer the reader to the original manuscript [20] for more information on the RND potential generation. To create datasets large enough to use DNNs, we chose to randomly sample k_i and x_{0_i} such that $0.01 \leq k_i \leq 0.16$ Ha/a_0^2 (Hartree per Bohr^2) and $-8.0 \leq x_{0_i} \leq 8.0$ a_0. With a given selection of these variables, the potential was then evaluated on a 40×40 a_0 parallelepiped with a 256×256 grid point mesh. We then chose to place either $N =1$, 2, 3, or 10 electrons in the 2D space. For each choice of the number of electrons, we generate an external potential, and then perform three DFT calculations, each with different exchange-correlation functionals. We used the local density approximation (LDA) exchange-correlation functional [21, 22], the Perdew-Burke-Ernzerhof (PBE) [23] functional for exchange and the LDA correlation functional, and the meta-generalized gradient approximation (MGGA) exchange functional from Pittalis *et al.* [24] and the LDA correlation functional. All of the calculations were carried in real space with the Octopus code [25, 26, 27]. For testing, we set aside 10% of each data set. This made for 90,000 training configurations and 10,000 testing configurations for each case of potential, number of electrons, and exchange-correlation functional. The calculations are summarized in Table 1 of the supplementary information.

When constructing the EDNNs, we used a mixture of Tensorflow [28] and TFlearn [29] in Python. For the networks topologies we build on our previous reports [16, 19] and use EDNNs where each tile of the EDNN has the same in-tile CNN used previously for predicting KS-DFT total energies of 2D hexagonal sheets [16]. For clarity, the in-tile CNN consisted of 2 reducing convolutional layers with kernel sizes of 3, 6 non-reducing convolutional layers with kernel sizes of 4, 1 reducing convolutional layer with a kernel size of 3, 4 non-reducing convolutional layers with kernel sizes of 3, a fully connected layer with 1024 neurons, and a final fully connected layer with one neuron. All of

the activations used were rectified linear units. We emphasize that in our approach, we do not do any sort of feature engineering, like past reports that use artificial neural networks [7, 6, 5, 4, 3, 2, 14]. The convolutional layers in the EDNNs identify relevant features during the training process. When utilizing an EDNN, one must declare the focus and context regions which is used to "tile" up the image into fragments. To find the ideal focus and context regions, we started by training the EDNNs on the 2D charge density to total energy mapping as well as the 2D external potential to total energy mapping for the 1, 2, 3, and 10 electron systems for calculations done with the LDA exchange-correlation functional. We chose a variety of focus and context sizes, and found that the optimal focus and context sizes are 128 pixels for the focus size, and 32 pixels for the context size. Our decision was based on a balance between accuracy and computation time. A larger focus size lowers the computation time, and a larger context size yields larger images, resulting in more neurons in the EDNNs thereby improving the accuracy of the model. For a focus of 128 pixels, we found that the accuracies were very similar for various context sizes and the choice of 32 pixels was almost arbitrary. While training, we used a learning rate of 10^{-4} for 500 epochs when using the charge densities as input and a learning rate of 10^{-5} for 500 epochs when using the external potentials as input. In both cases, we further reduced the learning rates by a factor of 10 and trained for an additional 100 epochs.
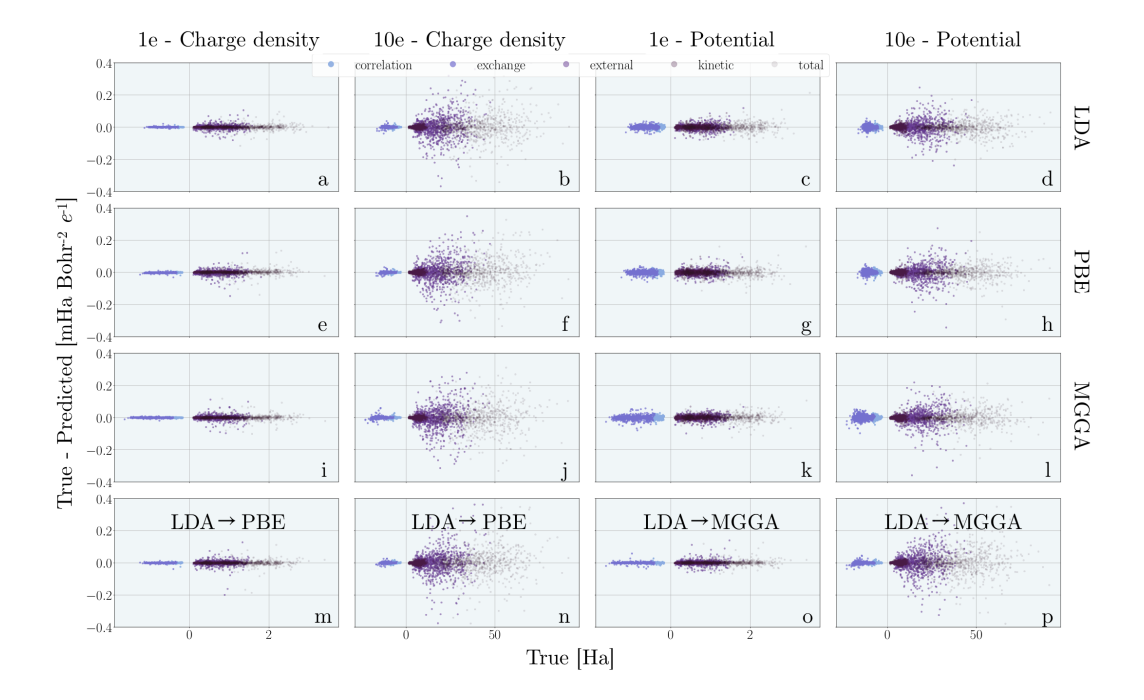
Figure 3: True minus predicted (in mHa / Bohr^2) versus true (Ha) for various models with the RND potentials. Plots a-d are models trained with the LDA exchange-correlation functional, e-f with the PBE exchange-correlation functional, and i-l with the MGGA exchange-correlation functional. First column (a, e, i) is for 1 electron models where the charge densities were used as input. Second column (b, f, j) is for 10 electron models where the charge densities were used as input. Third column (c, g, k) is for 1 electron models where the external potentials were used as input. Fourth column (d, h, l) is for 10 electrons models where the external potentials were used as input. The bottom row (m-p) is for models where LDA charge densities were used as input, and the labels were either PBE energies (m, n) or MGGA energies (o, p). Plots m, o are for the 1 electron systems, and n, p for the 10 electron systems. It should be noted that one model is predicting the correlation, exchange, external, kinetic, and total energies.

5

3 Results

3.1 Energy predictions

3.1.1 EDNNs as a functional

Firstly, we show that EDNNs can be used as an energy functional for correlation, exchange, external, kinetic and total energies. For the LDA, PBE, and MGGA functionals discussed in Section 2, we used the computed self-consistent charge densities as input to an EDNN and were able to successfully predict the correlation, exchange, external and total energies simultaneously for both SHO and RND external potentials. Starting with the models where the SHO external potentials were used in the DFT calculations, we found that the mean absolute errors for each particular case are within chemical accuracy. These can be seen in Table 3 of the supplementary information. In Figure 3, we show predicted minus true versus true for the one and ten electron models with the different exchange-correlation functionals when the RND external potentials were used in the DFT calculations. In this figure, it is clear that the error of the models increase with the number of electrons. This increase in error is expected due to the increase in the range of energies and can be physically attributed to the increase of interactions in the system. Looking to Table 2 of the supplementary information we also observe that mean absolute errors become larger as the complexity of the exchange-correlation functional increases. In addition to these trends, we also notice that the energy with the largest mean absolute error comes from the external energy functional. This again can be attributed to the ranges of the various energies. The external energy has the largest range out of all the energies being predicted.

DFT is a more popular choice for larger systems relative to wavefunction based methods because the exchange-correlation functionals used are computationally inexpensive relative to methods that employ exact exchange, for example. In light of this, we have trained EDNNs to predict energies at the PBE and MGGA level given a self-consistent charge density computed with the LDA exchange-correlation functional. In Figure 3, we show true minus predicted versus true for 1 and 10 electron models trained on the mapping between LDA charge densities and either PBE or MGGA energies. Similar to the results mentioned above, the mean absolute errors increase both with the number of electrons and the complexity of the exchange-correlation functional. In Table 2 of the supplementary information, we also notice that the highest mean absolute error is for the external and total energies. This result further suggests that there is not a fundamental problem with learning the external energy, but the larger range of energies makes it more difficult for a EDNN to handle with extreme precision. The success of learning the energies of a more accurate exchange-correlation functional given a less accurate charge density shows promise for other applications. A future application could include learning a G_0W_0 total energy from a DFT computed self-consistent charge density, similar to the work that was completed by Kolb *et al.* [14].

A note should be made about Table 2 with respect to the magnitude of some of the mean absolute errors reported. In comparison to the report by Mills *et al.* [20], some of the mean absolute errors are larger by some cases a factor of 10. This could be attributed to: the differences in amount of data used, the differences in the number of epochs, the range of energies, uniform versus non-uniform distribution of energies, or training on a single energy rather than multiple energies simultaneously. In the work of Mills *et al.*, they used 200,000 training examples and trained for 1000 epochs. For the RND potentials, they also trained a model for an additional 2000 epochs and used an additional 200,000 training examples (for a total of 400,000 training examples) which gave them a 30% reduction of their error. When we doubled the size of our training sets, we found a 15% reduction of the mean absolute errors for the 1 electron systems with the MGGA functional and the RND external potentials. To further reduce the magnitudes of the mean absolute errors, we then considered the importance of energy sampling. In previous reports [15, 20, 16], uniform sampling has shown to decrease the error of machine learning models. We found after uniformly sampling the total energy for the 10 electron system with the RND external potentials and the MGGA functional that the mean absolute errors dropped by a factor of ~ 2. Lastly, we considered the range of energies in our dataset. For the 10 electron systems with SHO and RND external potentials, the total energy range is roughly 15 Ha (~ 400 eV) and 100 Ha (~ 2700 eV). Such energy ranges are several orders of magnitude larger than previous reports [15, 20, 16]. The differences in accuracy between the SHO external potentials and RND external potentials are due to the differences in energy ranges and complexities. The RND potentials have a larger range and much more complex curvature than the SHO external potentials.

The absolute values of DFT total energies are meaningless. It is more meaningful to calculate energy differences between different configurations (i.e. adsorption or binding energies) with DFT to see if a structure or bond is energetically favourable. To address this, we compared the true energy differences between configurations with the predicted energy differences between configurations across our entire test sets. For the SHO external potentials, we find that the mean absolute error of the energy differences are all within chemical accuracy. For the RND external potentials, the error of the energy differences are slightly larger than the mean absolute errors of the energy predictions and they follow the same trend as the mean absolute errors of the energy predictions. These can be seen in Tables 2 and 3.

3.1.2 Circumventing Kohn-Sham DFT

In addition to using EDNNs as a functional, it is arguably more convenient to train a EDNN to learn the mapping between the external potential and the contributing energies of that system. It is more convenient because it avoids calculating a self-consistent charge density with the Kohn-Sham scheme. We have trained EDNNs to predict the exchange, correlation, external, kinetic, and total energy simultaneously using the external potential as input rather than the charge density. Again, in Figure 3 we show true minus predicted versus true for the correlation, exchange, external, kinetic, total energies for the RND external potentials. Here, it is evident that the charge density is more optimal as an input to a EDNN for 1 electron as there is much more spread in the distribution. For 10 electrons, this is not the case. Looking to Table 2, we can see that for 1, 2, and 3 electrons no matter what choice of exchange-correlation functional, the charge density is a more appropriate choice as input to a EDNN for predicting the energies. The mean absolute errors are lower for all energies. In the case of 10 electrons, the mean absolute errors in the external and total energies are lower for the models that have potentials as input. Although the errors are lower for the external and total energies, the mean absolute errors for correlation, exchange, and kinetic energies are larger. When training a model on a set of energies, there is a balance between the errors of the energies since the loss function depends on the sum over the mean squared errors between the true and predicted energies. In the case of using charge densities as input to the EDNN, we found a local minima where the exchange, correlation, and kinetic energies can be predicted with much better accuracy than the external or total energies. In the case of using potentials as input to the EDNN, we found that there is more of a balance of accuracy between the different energies being predicted. When examining the mean absolute errors of the true and predicted energy differences between configurations there is no obvious trend, but all of the values are well within chemical accuracy when using the SHO external potentials. Again, the differences in accuracies between the SHO and RND external potentials can be attributed to the increased energy ranges and increased complexity of the RND potentials. For the SHO external potentials, the EDNNs are capable to handle energy differences between configurations to within chemical accuracy. Like the charge density models, an EDNN trained with the external potentials as input would have the ability to calculate adsorption or binding energies. This would make for an even more rapid screening process of adsorption sites since the diagonalization of the Kohn-Sham Hamiltonian is avoided.

3.2 Image predictions

In both KS-DFT and OF-DFT, the self-consistent charge density is the central quantity that one is interested in calculating. Once one has the charge density, most other quantities can be calculated in a straightforward manner. In this Subsection, we address the viability of using DCIGNs to map the external potential to the self-consistent charge density in 2D for the RND potentials with the LDA, PBE, and MGGA exchange correlation functionals. DCIGNs were recently introduced in the literature [30] and have a similar topology to autoencoders. The DCIGN that we have used has 4 reducing convolutional layers, 3 non-reducing convolutional layers, and 4 deconvolutional layers such that the output image has the same dimensionality as the input image. This topology differs slightly from the original work on DCIGNs [30], where a fully connected layer would replace our 3 non-reducing convolutional layers. All of our convolutional layers use a kernel size of 3 with rectified linear unit activations. We used a learning rate of 10^{-5} while training for 500 epochs and dropped the learning rate by a factor of 10 before training for an additional 100 epochs. For this discussion we focus solely on the 10 electron calculations with the RND external potentials. We argue that these are the most challenging calculations to train with a DCIGN, and can therefore safely assume that the less complex calculations would be successful given the success of the most complex cases. In
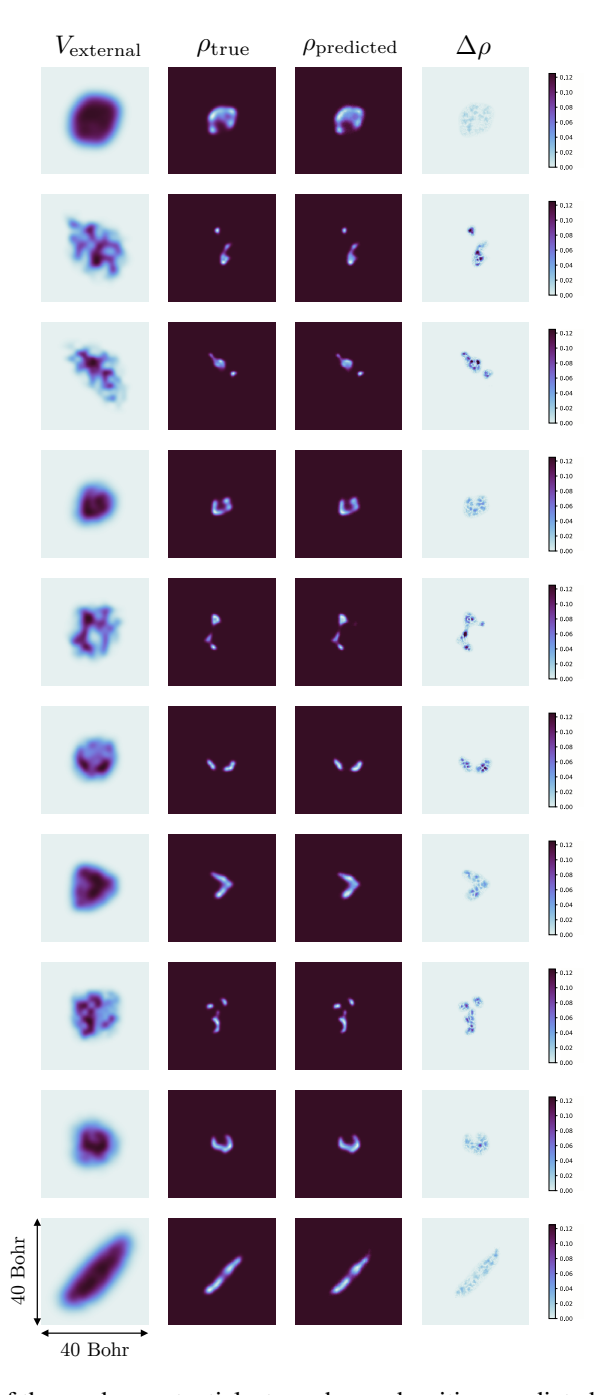
Figure 4: Examples of the random potentials, true charge densities, predicted charge densities, and differences between the true and predicted charge densities. The charge densities shown here were computed with the LDA exchange-correlation functional.

Figure 4, we show some of the predictions that the DCIGN made for 10 electrons calculations with the LDA exchange-correlation functional. There is a remarkable resemblance between the true and predicted charge densities. The DCIGN is capable of handling the extreme variability of the complex shapes, and is capable of handling the cases where the charge density is not isolated to one region of space. From a qualitative perspective, the DCIGN makes accurate predictions of the charge densities given RND external potentials.

Normally, when addressing the viability of a machine learning model from a quantitative perspective one considers the mean absolute error on the test set. We argue that a more rigorous test for the predicted charge densities would be mean absolute error of the energies associated with the predicted charge densities. We therefore take the predicted charge densities and renormalize them such that $\int d\mathbf{r}\,\rho(\mathbf{r}) = 10$. Afterwards, we use the renormalized predicted charge densities as input to subset of the models described in Subsection 3.1.1. We then compare the energies predicted from the predicted charge densities with the true energies. In Table 2, we show the mean absolute errors between the true and predicted energies as well as the mean absolute errors between the true energy differences and the predicted energy differences between configurations. When comparing the mean absolute errors of and predicted energies for the predicted charge densities with the energy predictions made from the true charge densities, the minimal difference was seen for the correlation energies with a value of ~ 6 mHa. The maximal difference between the mean absolute errors when comparing the energy predictions of the true and predicted charge densities was the total energy which was ~ 20 mHa.

4   Conclusion

In conclusion, we have shown that EDNNs and DCIGNs can be used alongside, or replace conventional KS-DFT calculations. When considering the SHO external potentials, EDNNs have the capability to make energy predictions using both the charge densities and the external potentials as input for correlation, exchange, external, kinetic and total energy simultaneously to within chemical accuracy. When considering the RND external potentials, the majority of the mean absolute errors of the energy predictions when using the both the charge density and external potentials as input are above chemical accuracy at most by an order of magnitude. When using DCIGNs, we have shown that they qualitatively reproduce the charge density, even for the complex RND potentials. In addition, in all cases considered in this report we found that the absolute errors between the true energy differences and predicted energy differences between configurations are all within chemical accuracy for the SHO external potentials. The results of this report show promise for future application in two regards. First, that this framework has the capability to make predictions of higher level theory calculations given a lower level theory charge density similar to a previous report [14]. Second, EDNNs can be used to calculate energy differences between structures to a high level of accuracy. This means that one can rapidly screen for stable adsorption sites or energetically favourable structures enhancing a new materials discovery process.

5   Acknowledgements

References

[1] Walter Kohn and Lu Jeu Sham. Self-consistent equations including exchange and correlation effects. *Physical review*, 140(4A):A1133, 1965.

[2] Jörg Behler. Neural network potential-energy surfaces in chemistry: a tool for large-scale simulations. *Physical Chemistry Chemical Physics*, 13(40):17930–17955, 2011.

[3] Sönke Lorenz, Axel Groß, and Matthias Scheffler. Representing high-dimensional potential-energy surfaces for reactions at surfaces by neural networks. *Chemical Physics Letters*, 395(4-6):210–215, 2004.

[4] Chris M. Handley and Paul L. A. Popelier. Potential energy surfaces fitted by artificial neural networks. *The Journal of Physical Chemistry A*, 114(10):3371–3383, 2010. PMID: 20131763.

[5] Roman M. Balabin and Ekaterina I. Lomakina. Neural network approach to quantum-chemistry data: Accurate prediction of density functional theory energies. *The Journal of Chemical Physics*, 131(7):074104, 2009.

[6] Jörg Behler and Michele Parrinello. Generalized neural-network representation of high-dimensional potential-energy surfaces. *Phys. Rev. Lett.*, 98:146401, Apr 2007.

[7] Changjian Xie, Xiaolei Zhu, David R. Yarkony, and Hua Guo. Permutation invariant polynomial neural network approach to fitting potential energy surfaces. iv. coupled diabatic potential energy matrices. *The Journal of Chemical Physics*, 149(14):144107, 2018.

[8] Kristof Schütt, Pieter-Jan Kindermans, Huziel Enoc Sauceda Felix, Stefan Chmiela, Alexandre Tkatchenko, and Klaus-Robert Müller. Schnet: A continuous-filter convolutional neural network for modeling quantum interactions. In *Advances in Neural Information Processing Systems*, pages 991–1001, 2017.

[9] Kristof T Schütt, Farhad Arbabzadah, Stefan Chmiela, Klaus R Müller, and Alexandre Tkatchenko. Quantum-chemical insights from deep tensor neural networks. *Nature communications*, 8:13890, 2017.

[10] John C Snyder, Matthias Rupp, Katja Hansen, Klaus-Robert Müller, and Kieron Burke. Finding density functionals with machine learning. *Physical review letters*, 108(25):253002, 2012.

[11] Li Li, Thomas E. Baker, Steven R. White, and Kieron Burke. Pure density functional for strong correlation and the thermodynamic limit from machine learning. *Phys. Rev. B*, 94:245129, Dec 2016.

[12] Li Li, John C. Snyder, Isabelle M. Pelaschier, Jessica Huang, Uma-Naresh Niranjan, Paul Duncan, Matthias Rupp, Klaus-Robert Müller, and Kieron Burke. Understanding machine-learned density functionals. *International Journal of Quantum Chemistry*, 116(11):819–833, 2016.

[13] John C. Snyder, Matthias Rupp, Katja Hansen, Leo Blooston, Klaus-Robert Müller, and Kieron Burke. Orbital-free bond breaking via machine learning. *J. Chem. Phys.*, 139:224104, 2013.

[14] Brian Kolb, Levi C. Lentz, and Alexie M. Kolpak. Discovering charge density functionals and structure-property relationships with prophet: A general framework for coupling machine learning and first-principles methods. *Scientific Reports*, 7(1), 4 2017.

[15] Felix Brockherde, Leslie Vogt, Li Li, Mark E Tuckerman, Kieron Burke, and Klaus-Robert Müller. By-passing the kohn-sham equations with machine learning. *Nature Communications*, 8, 2016.

[16] Kevin Ryczko, Kyle Mills, Iryna Luchak, Christa Homenick, and Isaac Tamblyn. Convolutional neural networks for atomistic systems. *Computational Materials Science*, 149:134–142, 2018.

[17] Pierre Hohenberg and Walter Kohn. Inhomogeneous electron gas. *Physical review*, 136(3B):B864, 1964.

[18] Kun Yao and John Parkhill. Kinetic energy of hydrocarbons as a function of electron density and convolutional neural networks. *Journal of chemical theory and computation*, 12(3):1139–1147, 2016.

[19] Iryna Luchak, Kyle Mills, Kevin Ryczko, Adam Domurad, and Isaac Tamblyn. Extensive deep neural networks. *arXiv preprint arXiv:1708.06686*, 2017.

[20] Kyle Mills, Michael Spanner, and Isaac Tamblyn. Deep learning and the schrödinger equation. *Phys. Rev. A*, 96:042113, Oct 2017.

[21] P. A. M. Dirac. Note on exchange phenomena in the thomas atom. *Mathematical Proceedings of the Cambridge Philosophical Society*, 26(3):376–385, 1930.

[22] m F Bloch. Bemerkung zur elektronentheorie des ferromagnetismus und der elektrischen leitfähigkeit. *Zeitschrift für Physik A Hadrons and Nuclei*, 57(7):545–555, 1929.

[23] John P Perdew, Kieron Burke, and Matthias Ernzerhof. Generalized gradient approximation made simple. *Physical review letters*, 77(18):3865, 1996.

[24] S Pittalis, E Räsänen, N Helbig, and EKU Gross. Exchange-energy functionals for finite two-dimensional systems. *Physical Review B*, 76(23):235314, 2007.

[25] Xavier Andrade, David Strubbe, Umberto De Giovannini, Ask Hjorth Larsen, Micael JT Oliveira, Joseba Alberdi-Rodriguez, Alejandro Varas, Iris Theophilou, Nicole Helbig, Matthieu J Verstraete, et al. Real-space grids and the octopus code as tools for the development of new simulation approaches for electronic systems. *Physical Chemistry Chemical Physics*, 17(47):31371–31396, 2015.

[26] Xavier Andrade, Joseba Alberdi-Rodriguez, David A Strubbe, Micael JT Oliveira, Fernando Nogueira, Alberto Castro, Javier Muguerza, Agustin Arruabarrena, Steven G Louie, Alán Aspuru-Guzik, et al. Time-dependent density-functional theory in massively parallel computer architectures: the octopus project. *Journal of Physics: Condensed Matter*, 24(23):233202, 2012.

[27] Xavier Andrade and Alán Aspuru-Guzik. Real-space density functional theory on graphical processing units: computational approach and comparison to gaussian basis set methods. *Journal of chemical theory and computation*, 9(10):4360–4373, 2013.

[28] Martín Abadi, Paul Barham, Jianmin Chen, Zhifeng Chen, Andy Davis, Jeffrey Dean, Matthieu Devin, Sanjay Ghemawat, Geoffrey Irving, Michael Isard, et al. Tensorflow: A system for large-scale machine learning. In *OSDI*, volume 16, pages 265–283, 2016.

[29] Yuan Tang. Tf. learn: Tensorflow's high-level module for distributed machine learning. *arXiv preprint arXiv:1612.04251*, 2016.

[30] Tejas D Kulkarni, William F. Whitney, Pushmeet Kohli, and Josh Tenenbaum. Deep convolutional inverse graphics network. In C. Cortes, N. D. Lawrence, D. D. Lee, M. Sugiyama, and R. Garnett, editors, *Advances in Neural Information Processing Systems 28*, pages 2539–2547. Curran Associates, Inc., 2015.

A   More details on the generated data

Dimension	N	V_{ext}	$V_X + V_C$	Number of calculations
2D	1	SHO	LDA + LDA	100,000
2D	1	SHO	PBE + LDA	100,000
2D	1	SHO	mGGA + LDA	100,000
2D	1	RND	LDA + LDA	100,000
2D	1	RND	PBE + LDA	100,000
2D	1	RND	mGGA + LDA	100,000
2D	2	SHO	LDA + LDA	100,000
2D	2	SHO	PBE + LDA	100,000
2D	2	SHO	mGGA + LDA	100,000
2D	2	RND	LDA + LDA	100,000
2D	2	RND	PBE + LDA	100,000
2D	2	RND	mGGA + LDA	100,000
2D	3	SHO	LDA + LDA	100,000
2D	3	SHO	PBE + LDA	100,000
2D	3	SHO	mGGA + LDA	100,000
2D	3	RND	LDA + LDA	100,000
2D	3	RND	PBE + LDA	100,000
2D	3	RND	mGGA + LDA	100,000
2D	10	SHO	LDA + LDA	100,000
2D	10	SHO	PBE + LDA	100,000
2D	10	SHO	mGGA + LDA	100,000
2D	10	RND	LDA + LDA	100,000
2D	10	RND	PBE + LDA	100,000
2D	10	RND	mGGA + LDA	100,000
total				2,400,000

Table 1: Summary of the calculations that were used for training and testing the deep learning models. N is the number of electrons, V_{ext} is the external potential chosen (see text), and $V_X + V_C$ are the exchange-correlation potentials chosen.

B   Results with the random external potentials

$N_{electrons}$	Input	Functional	$E_{correlation}$	$\Delta E_{correlation}$	$E_{exchange}$	$\Delta E_{exchange}$	$E_{external}$	$\Delta E_{external}$	$E_{kinetic}$	$\Delta E_{kinetic}$	E_{total}	ΔE_{total}
1	2D - CD	LDA	0.89	0.120	1.42	0.095	14.49	0.437	2.46	0.204	14.47	0.061
2	2D - CD	LDA	1.14	0.066	1.78	0.064	9.61	0.099	2.25	0.026	9.95	0.088
3	2D - CD	LDA	1.97	0.065	3.05	0.062	35.14	0.305	5.619	0.063	36.10	0.117
10	2D - CD	LDA	1.96	0.017	3.02	0.018	73.42	0.198	6.65	0.021	74.38	0.109
1	2D - CD	PBE	1.91	0.848	3.15	0.667	15.32	0.867	3.80	0.300	15.15	0.750
2	2D - CD	PBE	1.33	0.006	1.93	0.001	9.49	0.266	2.24	0.027	10.07	0.113
3	2D - CD	PBE	1.97	0.019	2.92	0.017	34.43	0.142	5.17	0.030	35.56	0.025
10	2D - CD	PBE	1.90	0.030	2.85	0.025	73.68	0.174	7.56	0.025	74.99	0.107
1	2D - CD	MGGA	1.03	0.125	2.10	0.159	13.70	0.776	2.51	0.110	13.87	0.301
2	2D - CD	MGGA	1.25	0.010	2.55	0.001	9.98	0.041	2.44	0.049	10.19	0.001
3	2D - CD	MGGA	1.76	0.064	3.59	0.060	34.11	0.076	4.73	0.095	36.46	0.047
10	2D - CD	MGGA	2.20	0.030	4.45	0.032	77.15	0.181	7.32	0.007	78.51	0.101
1	2D - POT	LDA	5.33	0.223	8.55	0.163	17.80	0.167	11.51	0.075	22.31	0.004
2	2D - POT	LDA	5.34	0.135	8.46	0.212	18.47	0.233	8.78	0.070	21.22	0.073
3	2D - POT	LDA	10.57	0.033	16.77	0.039	46.17	0.023	15.76	0.103	43.22	0.067
10	2D - POT	LDA	6.63	0.002	10.30	0.009	50.30	0.004	10.48	0.002	40.89	0.002
1	2D - POT	PBE	6.03	0.035	9.29	0.191	17.24	0.208	12.09	0.269	22.48	0.274
2	2D - POT	PBE	5.96	0.226	8.99	0.294	19.51	0.106	10.04	0.046	21.34	0.066
3	2D - POT	PBE	10.89	0.035	16.79	0.053	46.13	0.176	16.34	0.070	43.59	0.043
10	2D - POT	PBE	7.14	0.063	10.78	0.061	49.26	0.009	10.38	0.025	39.44	0.007
1	2D - POT	MGGA	5.70	0.061	11.96	0.081	16.15	0.207	10.89	0.223	21.66	0.069
2	2D - POT	MGGA	5.35	0.033	11.03	0.012	14.80	0.007	8.09	0.097	19.26	0.118
3	2D - POT	MGGA	11.07	0.108	22.92	0.081	44.54	0.047	16.68	0.075	42.97	0.042
10	2D - POT	MGGA	7.31	0.047	15.05	0.042	50.78	0.004	10.78	0.026	41.38	0.007
1	2D - CD	LDA→PBE	1.18	0.075	1.74	0.056	14.49	0.638	2.42	0.105	14.62	0.150
2	2D - CD	LDA→PBE	1.24	0.051	1.84	0.038	8.61	0.060	1.94	0.012	9.10	0.056
3	2D - CD	LDA→PBE	1.91	0.003	2.78	0.009	34.76	0.0175	5.08	0.001	35.59	0.054
10	2D - CD	LDA→PBE	2.16	0.027	3.23	0.031	75.50	0.170	7.59	0.007	76.72	0.105
1	2D - CD	LDA→MGGA	1.39	0.165	2.90	0.142	14.22	0.711	2.63	0.039	14.73	0.253
2	2D - CD	LDA→MGGA	1.47	0.033	2.99	0.040	7.96	0.208	1.98	0.091	8.67	0.125
3	2D - CD	LDA→MGGA	2.88	0.104	5.99	0.106	36.29	0.214	5.78	0.174	37.71	0.097
10	2D - CD	LDA→MGGA	2.60	0.032	5.31	0.033	73.58	0.175	7.50	0.013	74.40	0.101
10	2D - PCD	LDA	6.35	0.230	9.90	0.232	93.00	0.074	12.66	0.250	98.86	0.066
10	2D - PCD	PBE	7.19	0.204	10.85	0.199	100.37	0.006	14.54	0.249	108.07	0.138
10	2D - PCD	MGGA	7.51	0.324	15.36	0.322	94.55	0.135	12.99	0.388	103.28	0.259

Table 2: Mean absolute errors and energy differences between configurations (in mHa per electron) for models trained in this report for the RND potentials. The abbreviations CD, POT, and PCD are charge density, potential, and predicted charge density respectively. The arrows (i.e. LDA→PBE) indicate that the charge density used as input to the DNN was calculated using the LDA exchange-correlation functional, but the labels (energies) were calculated using another exchange-correlation functional.

C   Results with the simple harmonic oscillator external potentials

$N_{electrons}$	Input	Functional	$E_{correlation}$	$\Delta E_{correlation}$	$E_{exchange}$	$\Delta E_{exchange}$	$E_{external}$	$\Delta E_{external}$	$E_{kinetic}$	$\Delta E_{kinetic}$	E_{total}	ΔE_{total}
1	2D-CD	LDA	0.072	0.034	0.116	0.037	0.087	0.001	0.081	0.006	0.179	0.030
2	2D-CD	LDA	0.085	0.066	0.138	0.064	0.112	0.099	0.086	0.026	0.269	0.088
3	2D-CD	LDA	0.087	0.038	0.145	0.036	0.197	0.012	0.145	0.016	0.471	0.025
10	2D-CD	LDA	0.099	0.001	0.156	0.001	0.346	0.003	0.178	0.004	0.886	0.005
1	2D-CD	PBE	0.098	0.233	0.160	0.237	0.119	0.143	0.107	0.149	0.227	0.126
2	2D-CD	PBE	0.106	0.075	0.161	0.066	0.119	0.002	0.099	0.041	0.282	0.031
3	2D-CD	PBE	0.136	0.018	0.215	0.034	0.307	0.032	0.167	0.064	0.772	0.020
10	2D-CD	PBE	0.099	0.003	0.156	0.003	0.355	0.009	0.167	0.005	0.889	0.007
1	2D-CD	MGGA	0.095	0.271	0.200	0.259	0.135	0.267	0.120	0.245	0.276	0.280
2	2D-CD	MGGA	0.155	0.041	0.329	0.041	0.171	0.005	0.120	0.015	0.393	0.021
3	2D-CD	MGGA	0.104	0.029	0.213	0.023	0.157	0.003	0.115	0.006	0.382	0.006
10	2D-CD	MGGA	0.189	0.002	0.398	0.002	0.515	0.006	0.274	0.012	1.283	0.005
1	2D-POT	LDA	0.058	0.005	0.103	0.002	0.081	0.003	0.066	0.102	0.170	0.031
2	2D-POT	LDA	0.079	0.001	0.132	0.006	0.093	0.012	0.053	0.004	0.235	0.009
3	2D-POT	LDA	0.074	0.009	0.119	0.006	0.132	0.012	0.069	0.013	0.307	0.021
10	2D-POT	LDA	6.63	0.002	10.30	0.009	50.30	0.004	10.48	0.002	40.89	0.002
1	2D-POT	PBE	0.062	0.021	0.088	0.007	0.065	0.003	0.054	0.010	0.134	0.027
2	2D-POT	PBE	0.073	0.004	0.122	0.013	0.083	0.002	0.049	0.001	0.199	0.011
3	2D-POT	PBE	0.080	0.002	0.145	0.004	0.124	0.004	0.066	0.010	0.295	0.001
10	2D-POT	PBE	0.142	0.004	0.245	0.002	0.391	0.006	0.153	0.001	0.799	0.003
1	2D-POT	MGGA	0.052	0.044	0.121	0.006	0.063	0.009	0.051	0.033	0.151	0.029
2	2D-POT	MGGA	0.083	0.024	0.161	0.015	0.088	0.018	0.046	0.008	0.199	0.010
3	2D-POT	MGGA	0.087	0.014	0.193	0.005	0.135	0.018	0.077	0.004	0.343	0.016
10	2D-POT	MGGA	0.139	0.001	0.278	0.001	0.323	0.005	0.168	0.008	0.719	0.001
1	2D-CD	LDA→PBE	0.079	0.054	0.125	0.052	0.107	0.077	0.108	0.103	0.221	0.077
2	2D-CD	LDA→PBE	0.100	0.012	0.157	0.011	0.133	0.038	0.101	0.001	0.321	0.036
3	2D-CD	LDA→PBE	0.092	0.019	0.149	0.017	0.168	0.001	0.117	0.037	0.372	0.007
10	2D-CD	LDA→PBE	0.107	0.027	0.166	0.031	0.333	0.170	0.186	0.007	0.829	0.105
1	2D-CD	LDA→MGGA	0.090	0.041	0.196	0.043	0.132	0.041	0.126	0.093	0.262	0.009
2	2D-CD	LDA→MGGA	0.123	0.034	0.252	0.031	0.141	0.038	0.126	0.046	0.323	0.039
3	2D-CD	LDA→MGGA	0.128	0.013	0.273	0.016	0.214	0.035	0.157	0.043	0.521	0.037
10	2D-CD	LDA→MGGA	0.110	0.004	0.232	0.006	0.366	0.001	0.173	0.006	0.888	0.002

Table 3: Mean absolute errors and energy differences between configurations (in mHa per electron) for models trained in this report for the SHO potentials. The abbreviations CD, POT, and PCD are charge density, potential, and predicted charge density respectively. The arrows (i.e. LDA→PBE) indicate that the charge density used as input to the DNN was calculated using the LDA exchange-correlation functional, but the labels (energies) were calculated using another exchange-correlation functional.